Scientific Journal of King Faisal University:
Basic and Applied Sciences

# Acid Red 73 Removal By Chitosan/Ferrous Oxide Nanocomposite: Adsorption Behavior and Physicochemical Properties

**Khamael M. Abualnaja**
Department of Chemistry, College of Science, Taif University, Taif 21944, Saudi Arabia.

| LINK | RECEIVED | ACCEPTED | PUBLISHED ONLINE | ASSIGNED TO AN ISSUE |
|---|---|---|---|---|
| https://doi.org/10.37575/b/sci/250021 | 21/05/2025 | 31/07/2025 | 31/07/2025 | 01/12/2025 |
| **NO. OF WORDS** | **NO. OF PAGES** | **YEAR** | **VOLUME** | **ISSUE** |
| 7774 | 8 | 2025 | 26 | 2 |

## ABSTRACT

This study investigates the efficacy of a chitosan/ferrous oxide nanocomposite (CFON) for the elimination of the dye Acid Red-73 (AR73) from aqueous solutions. Physicochemical characterization via Fourier transform infrared spectroscopy confirmed the presence of critical functional groups (e.g., O-H/N-H stretch at ~3419 $cm^{-1}$, C-N stretch at ~1399 $cm^{-1}$, and Fe-O bond at ~642 $cm^{-1}$) integral to dye binding. Scanning electron microscopy revealed an uneven, irregular surface morphology with constituent nanoparticles in the 16–19.8 nm range, providing a substantial surface area for adsorption, while energy dispersive X-ray spectroscopy validated the elemental composition, notably carbon (39.76%), oxygen (38.13%), nitrogen (2.87%), and iron (0.54%). Batch adsorption experiments demonstrated exceptional CFON performance, achieving over 99% AR73 removal under optimized conditions (pH, adsorbent dose [0.02–0.04 g], contact time [120–240 min], and initial dye concentration [20–60 mg/L]). The adsorption equilibrium data were best described by the Freundlich isotherm model ($R^2$ = 0.958; KF = 1.048; 1/n = 6.234), indicating favorable multilayer adsorption onto a heterogeneous surface. Response surface methodology (RSM) with a central composite design identified the quadratic effect of contact time and the interaction between contact time and solution pH as the most statistically significant factors ($p < 0.05$ based on Pareto chart analysis).

**KEYWORDS**
Industrial pigments, multilayer adsorption, nanocomposite, removal efficiency, surface methodology, water pollution

**CITATION**
Abualnaja, K.M. (2025). Acid Red 73 removal by chitosan/ferrous oxide nanocomposite: Adsorption behavior and physicochemical properties. *Scientific Journal of King Faisal University: Basic and Applied Sciences*, **26**(2), 20–27. DOI: 10.37575/b/sci/250021

## 1. Introduction

Water pollution by pesticides, dyes, and heavy metals is a major environmental concern. Industrial effluents from paper, leather, and textile industries discharge persistent synthetic dyes that adversely affect aquatic ecosystems (Abdallah and Alprol, 2024). Among them, Acid Red 73 (AR73), a widely used azo dye, is highly toxic, mutagenic, and carcinogenic, posing serious risks to aquatic life and human health (Mansour *et al.*, 2022b). Conventional treatment methods, such as coagulation-flocculation, membrane filtration, and biological treatments, face limitations such as incomplete removal and high operational costs (Alprol, 2019). Therefore, the development of efficient and eco-friendly technologies for removing AR73 from wastewater is of great importance. Adsorption, however, offers a promising, cost-effective, and eco-friendly alternative for dye removal (Ghoneim *et al.*, 2014). The performance of this technique largely depends on the properties of the adsorbent material. In recent years, biopolymer-based nanocomposites have gained significant attention for wastewater treatment applications due to their biodegradability, renewability, and functional versatility. Ferrous oxide ($Fe_2O_3$) possesses several properties, including being a non-toxic, affordable, plentiful, and stable material with a sufficient bandgap of 2.2 eV. Exposure to visible light can activate this metal oxide, which is incredibly active (Mukherjee *et al.*, 2016; Ashour *et al.*, 2022). Ferrous oxide nanocomposite ($Fe_2O_3$ NPs) exhibit superparamagnetic properties and high chemical stability. In addition, chitosan, a naturally occurring biopolymer produced from chitin, has attracted a lot of interest as an adsorbent material because of its availability, biodegradability, and ability to adsorb a variety of contaminants. Due to their distinct electrical characteristics and capacity to produce reactive oxygen species when exposed to light, ferrous oxide nanoparticles have shown promise for the degradation of dyes (Preethi *et al.*, 2020; Alprol *et al.*, 2024).

A popular statistical method for developing tests, a regression model, assessing the influence of independent process factors, and identifying ideal conditions is the response surface methodology (RSM) approach. Using this method, an experimental matrix is created, the system's matching responses are found, and these two are fitted using the proper regression model (Karri and Sahu, 2018). Therefore, this study focuses on the de novo development of a chitosan/ferrous oxide nanocomposite (CFON) specifically engineered for the adsorptive removal of AR73 dye. While chitosan and iron oxides have been studied individually or in other composite forms, their combined application as CFON for targeting AR73 and the exploitation of their synergistic adsorptive effects for this specific dye constitutes a novel approach. A distinct contribution is the rigorous optimization of the CFON adsorption process for AR73 elimination using response surface methodology (RSM). This systematic statistical approach enables a comprehensive investigation of the interplay between critical process parameters (e.g., pH, adsorbent dosage, contact time, and initial dye concentration), leading to the identification of optimal conditions that maximize dye removal efficiency. This detailed, statistically guided optimization for the novel CFON-AR73 system represents a significant advancement beyond simple batch tests.

## 2. Materials and Methods

### 2.1. Preparation of the AR73 Dye Adsorbate:

The AR73 dye solution was prepared by dissolving one gram of AR73 dye powder in 1000 mL of distilled water to achieve the desired concentration (1000 mg/L). The pH of the solution might be adjusted using buffer solutions to achieve the desired pH level for the adsorption experiments. Among azo dyes, the chemical structure of AR73 dye is $C_{22}H_{14}N_4Na_2O_7S_2$.

### 2.2. Equipment:

Fourier transform infrared (FTIR) spectroscopy of the powder sample

Corresponding Author: Khamael M. Abualnaja 00966543362333, k.ala@tu.edu.sa

was acquired with a Bruker IFS 66v/S spectrometer (Germany) and an IR Affinity-1S-SHIMADZU spectrometer (Kyoto, Japan). Attenuated total reflection (ATR) was used to record FTIR spectra, with 32 scans in the 4000–400 1/cm spectral range and a resolution of 4 $cm^{-1}$. Additionally, SEM and EDX analysis, utilizing the JEOL JSM-IT200 equipment, were used to evaluate the form and elemental composition of the composite material constructed from chitosan. The picture has a magnification of 40,000x.

### 2.3. Preparation of CFON:

To dissolve 2 g of chitosan, a 100 mL solution of 2% acetic acid was used. Following full dissolution, the chitosan solution was thoroughly agitated with 2 mL of distilled water for two hours at 60 °C (Preethi *et al.*, 2020). After achieving a mildly alkaline solution, 0.1 M sodium hydroxide was added dropwise, and the mixture was allowed to gel completely for 48 hours. Demineralized water was used to wash the gel until it reached neutrality. After that, 50 mL of $Fe_2O_3$ solution was combined and agitated for 60 minutes at 60 °C. The mixture was then continuously stirred for two hours at 60 °C after 50 mL of chitosan solution was added. The prepared mixture was dropwise by adding 2 mL of glutaraldehyde (2.5%) to the prepared mixture (2.5 %) and continued stirring for 15 min, which acts as a catalyst and a cross-linking agent. To obtain the final product, the hydrogel was dried overnight at 80 °C to ensure complete evaporation of the water content.

### 2.4. Percentage Removal and Adsorption Capacities:

After the exposure period, the nanocomposite was separated from the dye solutions using filtration or centrifugation. Dye concentration was analyzed in the solutions treated using a UV-Vis spectrophotometer. After that, the dye concentration's adsorption capacity ($q_e$) and % elimination were determined. The concentration of AR73 dye was measured using spectrophotometry at $\lambda max$ = 510 nm. The experimental data were obtained from triplicate measurements (n = 3). The percentage removal and adsorption capacities ($q_e$) were estimated using the following equations (1 and 2) (Ashour *et al.*, 2023):

$$\text{AR73 Removal (\%)} = \frac{(Ci - Cf)}{Ci} \times 100$$

$$q_e = \frac{(Ci - Cf) \times V}{W}$$

Where: the concentration is represented by the symbols $C_i$ and $C_{f,\,which}$ are the liquid-phase concentrations of AR73 dye in mg/L at initial and equilibrium, respectively. In contrast, $q_e$ is the maximal adsorption at monolayer (mg/g). The mass of the adsorbent is (W) in grams, and the volume of the solution is V (L).

### 2.5. RSM Design Model:

To determine the precise external condition values that could lead to the highest removal efficiency, the RSM was utilised. As indicated in Table 1, three levels (-1, 0, and 1) were created by dividing the initial AR73 Concentration values of 20, 40, and 60 mg/L, the adsorbent dose levels of 0.02, 0.03, and 0.04 g, the sorption duration levels of 2, 3, and 4 hours, and the pH value levels of 3, 5, and 7. Using the Design Expert (v. 13) software, a total of 13 tests were simulated, with the response (Y) for each variable set to AR73 elimination efficiency.

**Table 1: The values of the coded factors, the levels of each variable, and the independent variables.**

| Variable | Symbol | -1 | 0 | +1 |
|---|---|---|---|---|
| Adsorbent dosage (g) | A | 0.02 | 0.03 | 0.04 |
| Contact Time (min) | B | 120 | 180 | 240 |
| pH | C | 3 | 5 | 7 |

To determine the model's fitness, the validity of the equations, and the importance of the response, ANOVA and residual values were employed. To determine the interactions between factors, the main effect plots and Pareto charts for each factor were examined. The specific impacts of each element were then ascertained using interaction effect plots, the Pareto chart, and 3D response surface plots. A central composite design was used to assess the four variables of contact duration, adsorbent dose, pH, and beginning dye concentration. Axial, Centre, and cube points are necessary for CCD. Equation (3) was used to get the total number of experiments (El-Naggar *et al.*, 2018).

$$N = 2k + 2k + C_0$$

Where K is the number of variables, $C_0$ is the Centre point's runs, 2k is the axial runs, and 2k is the cubic runs. As reported by Kasraee *et al.* (2023), the CCD was used for the development of mathematical equations. The empirical relationship between different dye removal (Y) and other parameters was determined with the following equation (4) (El-Naggar *et al.*, 2018):

$$Y = +42.49 - 8.91A + 16.14B + 1.85C - 18.83D + 2.05AB - 2.70AC + 1.26AD - 1.75BC - 1.27BD - 0.0969CD$$

## 3. Results and Discussion

### 3.1. Characterization of Adsorbent Composite:

#### 3.1.1. FTIR Analysis

For determining which functional groups are present in a molecule, FTIR spectroscopy is an essential analytical method. It works by measuring the absorption of infrared radiation by the sample at different wavelengths. Each functional group has a characteristic absorption pattern, allowing for the identification of various chemical bonds and compounds within the sample (Yan *et al.*, 2016). Figure 1A shows the results of an FTIR analysis for the CFON used in AR73 dye adsorption. The broad peak at 3419.476 $cm^{-1}$ (O-H -NH stretch) indicates the presence of hydroxyl and amine groups, likely from chitosan's polysaccharide structure and potentially adsorbed water molecules. These hydroxyl groups play a crucial role in hydrogen bonding with dye molecules, contributing significantly to the adsorption process. The band at 2076.421 $cm^{-1}$ suggests the presence of carbonyl groups (C=O stretch), possibly from aldehydes or ketones. The role of these groups in dye adsorption depends on the specific functional groups present in the AR73 molecule. Interactions could involve dipole-dipole interactions or hydrogen bonding with the dye. Meanwhile, the presence of carbon-carbon double bonds (C=C stretch) at 1637.312 $cm^{-1}$ is indicated, likely originating from aromatic rings or alkenes in the chitosan structure. These double bonds can interact with the aromatic rings often found in dye molecules through pi-pi interactions, further enhancing adsorption. The single peak at 1399.741 $cm^{-1}$ suggests the presence of amine groups (C-N stretch), which could potentially interact with specific functional groups present in the AR73 dye molecule, such as carboxylic acid or sulfonic acid groups, through electrostatic interactions or hydrogen bonding. Also, the peak at 1104.428 $cm^{-1}$ indicates the presence of C-O bonds, likely from alcohol or ether groups in the chitosan structure (Banerjee *et al.*, 2016). Like the O-H stretch, these groups can participate in hydrogen bonding with dye molecules. The peak of 642.691 $cm^{-1}$ confirms the presence of iron oxide (Fe-O bond) in the nanocomposite (Krishnan and Haridas, 2008). While not directly involved in dye binding, the Fe-O bond contributes to the overall surface properties of the nanocomposite, influencing its surface charge, porosity, and ultimately, its adsorption capacity. This implies that the ferrous oxide component, even at 0.54%, is not inert. Its primary role, according to this interpretation, is

to *modify* the chitosan matrix rather than acting as the main active site for dye binding itself.

The FTIR data show the presence of large amounts of amines (–NH2), hydroxides (–OH), phenolic acids (–CHOH), and carboxylic acids (–COOH), which may originate from the chitosan polymer.

#### 3.1.2. SEM Analysis

SEM analysis provides high-resolution images of a sample's surface topography and morphology, making it a popular method for characterizing nanomaterials and nanostructures (Akhtar *et al.*, 2018; Ashour *et al.*, 2023). This information is crucial for understanding the properties of nanomaterials and their potential applications (Alprol *et al.*, 2023). In the case of the CFON, SEM analysis can help confirm the presence of chitosan and ferrous oxide, as well as evaluate the size and dispersion of the nanoparticles within the composite. Figure 1B shows an uneven, irregular surface morphology, which is consistent with other reported SEM images of CFON. This type of surface morphology can provide a large surface area for adsorption, which is beneficial for applications such as removing dyes from water. The fact that the particle sizes are in the range of 16–19.8 nm is also promising for adsorption applications, as nanoparticles have a high surface area-to-volume ratio, which enhances their ability to adsorb pollutants. The surface morphology appears irregular and uneven, with some plate-like structures visible.

#### 3.1.3. EDX and Elemental Composition Analysis

SEM incorporates EDX technology. It detects the distinctive X-rays emitted when a sample is exposed to an electron beam, thereby identifying and quantifying the elemental composition of the sample (Fan *et al.*, 2009). These X-rays' energy levels match the elements found in the sample. The elemental composition and relative abundances of the observed X-rays are then ascertained. The data provided in Figure 1C show the elemental composition of the CFON, as analyzed using energy-dispersive X-ray spectroscopy (EDX). This analysis confirmed that carbon (C), with 39.76% of the mass, nitrogen (N), with 2.87% of the mass, and oxygen (O), with 38.13% of the mass, are the most abundant elements. The high C, N, and O content suggests the presence of chitosan in the composite. While the presence of iron (Fe) confirms the combination of ferrous oxide nanoparticles. However, the relatively low Fe content (0.54%) indicates a limited amount of iron oxide compared to chitosan. The 0.54% Fe confirms the 'nanocomposite' nature, but its low value reinforces that chitosan's properties will likely dictate the bulk of the adsorption behavior. The low Fe content (0.54%) in the CFON does not appear to be a detriment to its adsorption performance for AR73 dye within the context of this study. This is because chitosan, with its abundant hydroxyl and amine functional groups, serves as the primary workhorse for dye binding via mechanisms such as hydrogen bonding and electrostatic interactions. Its polymeric and porous nature inherently provides a high surface area. Also, the ferrous oxide nanoparticles, even in limited quantities, likely play a crucial *synergistic* and *modulatory* role rather than a primary direct binding role. They appear to enhance the overall surface area and porosity of the chitosan matrix by influencing its morphology and preventing chain aggregation. Modify the surface charge characteristics of the composite, potentially making it more favorable for AR73 adsorption. Contribute to the heterogeneity of the surface, consistent with the Freundlich isotherm. It's possible that this 0.54% loading represents a 'sweet spot' where the FeO NPs are well-dispersed and effectively modify the chitosan without negative effects, such as pore blockage or excessive aggregation, that might occur at higher FeO loadings. The study doesn't compare different FeO loadings, but the achieved performance suggests this level is effective. While aluminum (Al) and chlorine (Cl) elements might arise from impurities in the starting materials or the synthesis process. Ferrous oxide, chitosan, and a few other contaminants are confirmed to be present in the CFON by the EDX study.

### 3.2. RSM Model for Adsorptive Removal of AR73 Dye by CFON From Aqueous Solution:

#### 3.2.1. Analysis of Variance

To confirm the experimental design's statistical significance and determine the interactions between independent variables and response effects (Supplementary Tables 1 and 2), the ANOVA analysis was carried out as described by Karimifard and Moghaddam (2018). The experiment's approach actual outcomes, and the model-predicted AR 73 dye clearance rate (%) are shown in Table 2. According to the experimental findings, the clearance of AR 73 dye varied between 90% and 99%. The experiment likely investigates the influence of four factors (A, B, C, D) on the dye removal efficiency. Linear correlation $R^2$ =0.969 this indicates that the model explains 96.97% of the variability in the response (dye removal efficiency), suggesting a good fit. While adjusted $R^2$ (0.818): this considers the number of factors in the model and is more reliable than $R^2$ when comparing models with different numbers of factors. Furthermore, the signal-to-noise ratio is measured by adeq accuracy (7.4041), where a value higher than 4 is preferred. The value of 7.4041 indicates an acceptable signal, suggesting that the model can be utilized to explore the design space. The ANOVA analysis (Supplementary Tables 1 and 2) assists in assessing the significance of each factor and their interactions. Since this p-value is greater than 0.05, the model is not statistically significant. The model p-value (0.1424) indicates that the factors and their interactions do not significantly explain the variation in dye removal efficiency. Examining the p-values for A, B, C, and D, confirmed that none of them are less than 0.05. This implies that none of the individual factors has a statistically significant effect on dye removal efficiency. Similarly, the p-values for the interaction terms (AB, AC, AD, BC, BD, CD) are all greater than 0.05, suggesting that the interactions between the factors also do not significantly influence dye removal efficiency.

The mean dye removal efficiency across all experimental runs is 96.20. The standard deviation (1.45) represents the variability in the dye removal efficiency data. The coefficient of variation (CV = 1.51%) expresses the standard deviation as a percentage of the mean, indicating the relative variability in the data. Based on the presented analysis, although the model has a high $R^2$ value, the lack of statistical significance in the model and individual factors suggests that the RSM model may not be reliable for predicting dye removal efficiency within the experimental range.

**Figure 1: (A) FTIR analysis; (B) SEM analysis; (C) EDX analysis of the chitosan and ferrous oxide nanocomposite; (D) The standardized Pareto chart for AR73 dye adsorption by CFON adsorbent; the vertical line on the chart represents the significance threshold (at $\alpha = 0.05$).**

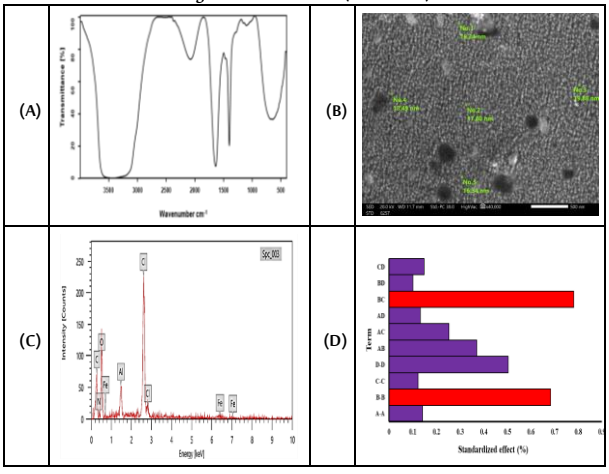

Table 2: AR73 elimination rates at each factor level are compared to experimental factor level values.

| Run | A: Adsorbent dosage (mg) | B: Contact Time (min) | C: pH | D: Initial AR73 concentration (mg/L) | AR73 Removal (%) |
|---|---|---|---|---|---|
| 1 | 1 | 1 | -1 | 0 | 99.93 |
| 2 | -1 | 0 | 1 | -1 | 91.04 |
| 3 | 0 | -1 | -1 | -1 | 93.75 |
| 4 | 0 | 1 | 1 | 1 | 99.91 |
| 5 | 1 | -1 | 1 | 1 | 97.74 |
| 6 | -1 | 1 | 0 | 1 | 99.96 |
| 7 | 1 | -1 | 0 | -1 | 96.86 |
| 8 | -1 | 1 | -1 | -1 | 99.96 |
| 9 | -1 | -1 | -1 | 1 | 92.63 |
| 10 | 1 | 0 | -1 | 1 | 90.88 |
| 11 | 0 | 0 | 0 | 0 | 97.73 |
| 12 | 1 | 1 | 1 | -1 | 94.27 |
| 13 | -1 | -1 | 1 | 1 | 95.9 |

The estimate of the coefficient indicates the change in response predicted for a one-unit change in factor value with all other variables held constant. In an orthogonal design, the intercept is the mean response over all runs. If the factors are orthogonal, the VIF is 1. A VIF > 1 indicates multi-collinearity, and the larger the VIF, the stronger the factor relationship. VIFs of less than 10 are generally acceptable (Supplementary Tables 1 and 2). High precision may be achieved in determining the signal-to-noise ratio. It should ideally be more than 4. A 7.404 ratio represents a good signal. This model may be used to traverse the design area. The model's F-value of 6.41 indicates that it is not significant, regardless of whether noise is present or not. This type of F-value is substantial and has a 14.24% chance of being caused by noise. P-values below 0.0500 indicate that the model terms are significant. Here, there aren't any important model terms. If the value exceeds 0.1000, the model terms are not important. The model may be improved by eliminating superfluous words (aside from those required to preserve hierarchy).

#### 3.2.2. Main Effect of Variables

The Pareto chart is a valuable tool for visualizing the significance of different factors and their interactions with the AR73 dye adsorption process. It helps identify the most influential parameters that affect removal efficiency. Based on the chart in Figure 1D, the factor with the most substantial impact on AR73 dye adsorption is BC (interaction between time and pH); this interaction has the highest standardized effect, indicating that the combined influence of contact time and pH significantly affects the removal efficiency. While B-B (time), the contact time itself also has a significant effect. Furthermore, the adsorption process is significantly influenced by dye's initial concentration, or D-D (initial dye concentration). AB (interaction between dosage and time): This interaction shows a moderate effect but does not exceed the significance threshold. Main Effects of A (dosage), C (pH), and D (initial dye concentration): Individually, these factors have relatively low standardized effects, suggesting that their influence might be more pronounced when interacting with other parameters.

### 3.3. Interactions of Various Factors on AR73 Removal:

#### 3.3.1. Interaction Between Adsorbent Dosage and Contact Time

Figure 2a presents the contour and 3D surface plots, which provide valuable insights into the interaction and influence of contact time and adsorbent dosage on the removal efficiency of AR73 dye by CFON adsorbent. Both plots reveal a clear trend that increasing both adsorbent dosage and contact time leads to higher dye removal efficiency. This indicates a synergistic effect between the two factors. The response surface plot shows a steeper gradient along the adsorbent dosage axis compared to the contact time axis. This suggests that changes in adsorbent dosage have a more pronounced impact on removal efficiency compared to changes in contact time, at least within the studied ranges (Ravulapalli and Kunta, 2019). As we move towards the higher end of the adsorbent dosage scale, the surface plot seems to flatten out, suggesting a plateauing effect. This implies that beyond a certain dosage, further increases might offer diminishing returns in terms of removal efficiency. Additionally, greater adsorption results from longer contact durations, as they enable more extensive interaction between the dye molecules and the adsorbent surface (Chueachot *et al.*, 2018). Higher adsorbent dosage provides a greater number of available binding sites for the dye molecules, enhancing the overall removal capacity. The saturation of the adsorbent's accessible binding sites may be the cause of the plateauing effect seen with increasing dose. Once most sites are occupied, adding more adsorbent has a limited impact on further removal.

#### 3.3.2. Interaction Between Adsorbent Dosage and pH

The contour and 3D response surface plots in Figure 2b illustrate the relationship between pH and adsorbent dose. Throughout the entire pH range, a discernible pattern of increasing removal efficiency with increasing adsorbent dosage is observed. However, the influence of pH appears more nuanced. The adsorption process of AR73 onto the CFON likely involves electrostatic interactions, which are influenced by pH. The optimal pH for dye removal might depend on the specific surface charge properties of the adsorbent and the dye molecules (Chaleshtori *et al.*, 2017).

#### 3.3.3. Interaction Between Adsorbent Dosage and Initial Dye Concentration

Figure 2c shows contour and 3D response surface plots for the initial AR73 dye concentration and adsorbent dosage. Increasing adsorbent dosage consistently leads to higher removal efficiency, especially at higher initial dye concentrations. The effect of initial dye concentration seems less pronounced at lower dosages. At low adsorbent dosages, the available binding sites might become saturated quickly with higher initial dye concentrations, limiting the overall removal efficiency. When sufficient adsorbents are available, higher initial dye concentrations can increase the driving force for adsorption, leading to a greater removal efficiency.

#### 3.3.4. Interaction Between Contact Time and pH

The pH and contact time contour plot and response surface plot are shown in Figure 3a. Increasing contact time generally enhances removal efficiency across the entire pH range studied. The influence of pH appears to be more complex. The adsorption process might require sufficient contact time for dye molecules to diffuse to the adsorbent surface and bind effectively. The rate of adsorption could be influenced by the pH level, potentially affecting the optimal contact time for different pH values. The response surface methodology (RSM) and ANOVA analyses were conducted to investigate the effects of variables such as contact time and pH on the adsorption process. While some interaction terms between variables were observed, statistical analysis showed that these interactions are not significant at the 95% confidence level ($p > 0.05$).

Therefore, the adsorption process appears to be mainly influenced by the individual effects of contact time and pH, rather than strong synergistic interactions between them. This finding suggests that optimization efforts should focus on controlling each variable independently to maximize adsorption efficiency.

#### 3.3.5. Interaction between contact time and initial dye concentration

Figure 3b shows the contour plot and response surface plot for the initial AR73 dye concentration and contact time. Longer contact times consistently improve removal efficiency, especially at higher initial dye concentrations. As in Figure 3b, the effect of initial dye concentration is less pronounced at shorter contact times. Achieving equilibrium between dye molecules in the solution and those adsorbed onto the surface might

require longer contact times, especially at higher initial concentrations (Putra *et al.*, 2014; Kareem *et al.*, 2021). At high concentrations, mass transfer limitations might slow down the adsorption process, necessitating longer contact times for efficient removal (Abualnaja *et al.*, 2021). Finally, Figures 2 and 3 illustrate the intricate interplay between various factors that affect dye removal efficiency. Optimization requires a comprehensive approach considering all relevant parameters and their interactions. Increasing adsorbent dosage consistently improves removal across different conditions, suggesting its importance in the process. The effects of pH and initial dye concentration appear more nuanced and might depend on the specific properties of the adsorbent and dye molecules. Utilizing RSM with a wider range of experimental conditions and factors can help develop a more robust model and identify the optimal conditions for dye removal efficiency while considering economic and practical constraints.

**Figure 2: The interactions of various factors on the removal of AR73 dye by the CFON, contour plots, 3D response surface plots; (a) the interaction of contact time and adsorbent dosage, (b) the interaction of pH and adsorbent dosage, and (c) the interaction of initial dye concentration and adsorbent dosage.**

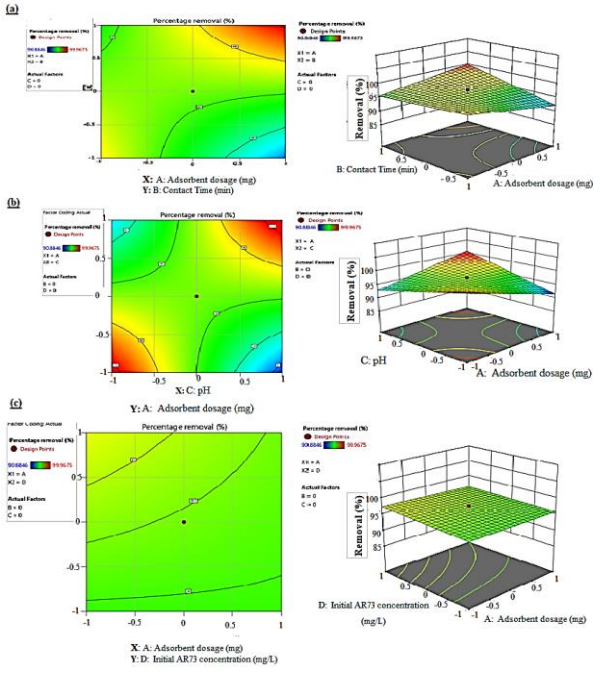


**Figure 3. The interactions of various factors on the removal of AR73 dye by the CFON, contour plots, 3D response surface plots; (a) the interaction between pH and contact time, (b) the interaction between initial dye concentration and contact time, and (c) the interaction between pH and initial dye concentration.**

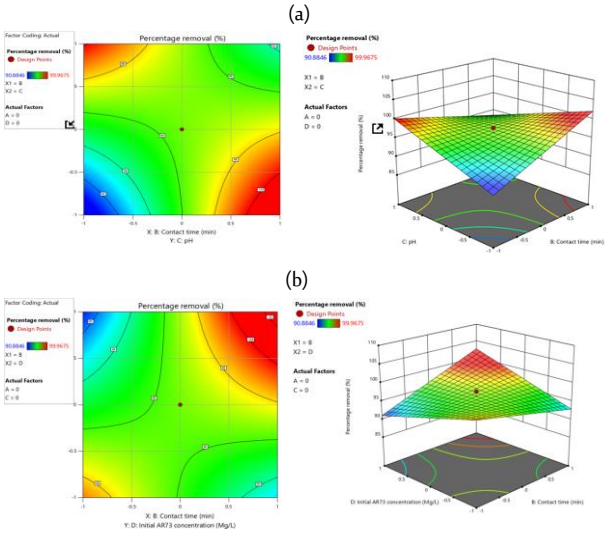


(c)

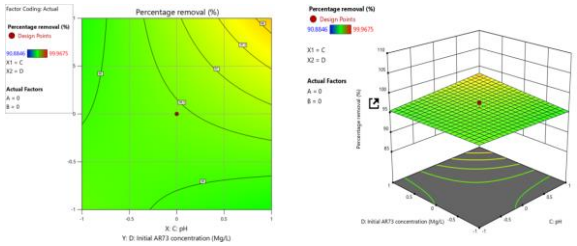


Nevertheless, the perturbation plot in Figure 4 shows the impact of each process variable on the removal efficiency of AR73 dye by the CFON adsorbent. Plot (A) suggests that decreasing the pH from its reference point (A = 0) leads to a decrease in dye removal efficiency. This is indicated by the downward slope of both the blue (B) and green (C, D) lines as they move towards the negative X-axis. A slight increase in pH above the reference point seems to have a minimal positive impact, as the lines are relatively flat on the positive X-axis side. Meanwhile, for residence time (B), increasing time (B) appears to have a positive impact on dye removal efficiency. This is evident from the upward slope of the blue line (B) as it moves towards the positive X-axis. Decreasing the residence time below the reference point seems to have a negative impact, as indicated by the downward slope of the line towards the negative X-axis. Plot (C) suggests that increasing the initial dye concentration from its reference point (C = 0) leads to a decrease in removal efficiency. This is indicated by the downward slope of both the green (C, D) and purple (C, D) lines as they move towards the positive X-axis. Decreasing the initial dye concentration below the reference point seems to have a positive impact, as indicated by the upward slope of the lines towards the negative X-axis. Like the initial dye concentration (D), increasing the adsorbent dosage from its reference point (D = 0) appears to have a negative impact on the removal efficiency. This is indicated by the downward slope of both the green (C, D) and purple (C, D) lines as they move towards the positive X-axis. Decreasing the adsorbent dosage below the reference point appears to have a positive impact, as indicated by the upward slope of the lines towards the negative X-axis.

**Figure 4: Effect of perturbation of each process variable.**

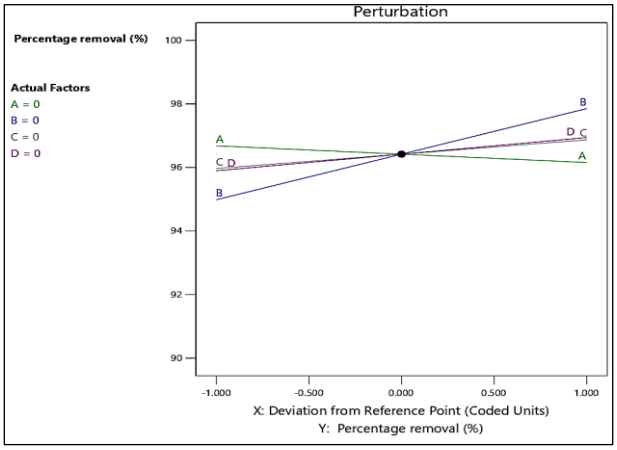


## 3.4. Analysis of Sorption Isotherms for AR73 Dye Removal:

This study investigates the adsorption behavior of AR73 dye onto a CFON using three isotherm models: Freundlich (Freundlich, 1906), Langmuir (Langmuir, 1916), and Harkins-Jura (Harkins and Jura, 1943) (the equations are presented in Supplementary Table 3). The values of the parameters obtained by fitting the data from adsorption trials to the linear versions of these models are presented in Supplementary Table 3. The Freundlich model describes multilayer adsorption on heterogeneous surfaces. The

values of 1/n (6.234) suggest favorable adsorption in both conditions (Mansour *et al.*, 2022a). The greater value indicates increased surface heterogeneity and the likelihood of a broader range of adsorption energies. Aside from that, this research prefers to draw on this isotherm equation in describing the chemical sorption process on an external surface, as the '1/n' component has a value larger than 1. Heterogeneity of sorption and positive binding are indicated whenever the n value for dye particles exceeds 1 (Salazar-Rabago *et al.*, 2017). Chelation, complexation, and ion exchange are forms of chemisorption, whereas physisorption refers to interactions mediated by electrostatic forces and van der Waals forces (Raval *et al.*, 2017).

Although the higher Kf value (1.048), it's significantly higher, indicating better adsorption efficiency. The good fit of the Freundlich model ($R^2 = 0.958$) suggests that it adequately describes the adsorption process and its heterogeneous nature (Figure 5). The Langmuir model assumes monolayer adsorption on a homogeneous surface. The data showed that the Qm values suggest a higher maximum adsorption capacity (357.14 mg/g) as shown in Supplementary Figure 1. The higher Ka value (435.54) indicates a stronger affinity between AR73 and the nanocomposite. The lower $R^2$ (0.657) values for the Langmuir model compared to the Freundlich model suggest that it is not as suitable for describing the adsorption process in this case. The Harkins-Jura model exhibits the poorest fit ($R^2 = 0.206$) among the three models, suggesting that it is not suitable for representing the adsorption process in this study (Supplementary Figure 2). Table 4 shows that the constants A and B parameters, which correspond to multilayer adsorption and heat of adsorption, respectively, reflect better adsorption energy and capacity. Unlike the Freundlich model, the Langmuir model in this instance shows greater correlation coefficients, reflecting a higher data fit. The Freundlich isotherm best describes the experimental data, as it verifies the heterogeneous nature of the adsorption process. Correspondingly, the Freundlich model appears to be the most suitable for describing the sorption equilibrium between AR73 dye and CFON nanoparticle with varying surface energies.

**Table 3: Isotherm parameters of isotherm models for AR73 dye by CFON antiparticle.**

| Isotherm Model | Isotherm Parameter | Value |
|---|---|---|
| Freundlich | 1/n | 6.234 |
| | $K_F$ ($mg^{1-1/n}L^{1/n}g^{-1}$) | 1.048 |
| | $R^2$ | 0.958 |
| Langmuir | $Q_m$ ($mg\ g^{-1}$) | 357.14 |
| | $K_a \times 10^3$ | 435.54 |
| | $R^2$ | 0.657 |
| Harkins-Jura isotherm | A | 2.42 |
| | B | 1.12 |
| | $R^2$ | 0.206 |

**Figure 5: Freundlich isotherm models for AR73 dye by CFON.**

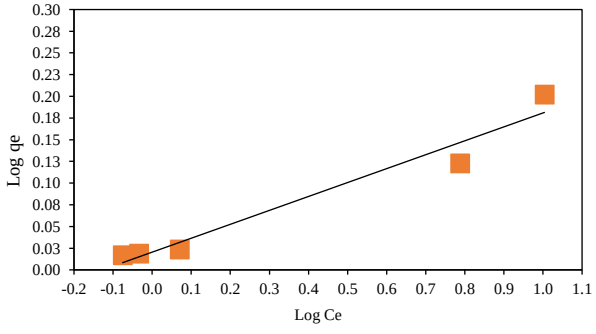


### 3.5. Effects of Temperature and Thermodynamic Study:

Figure 3S shows the effect of temperature on the adsorption efficiency of AR73 dye onto the CFON nanocomposite. The results indicate an evident inverse relationship between temperature and the removal efficiency of the dye by this nanocomposite. At 30 °C, it is approximately 85%–90% efficient in removal and raising the temperature to 60 °C results in a significant decrease in removal efficiency, approximately 30%. Such behavior indicates that the adsorption process is exothermic in nature; that is, increasing temperature will suppress the attraction forces between dye molecules and active sites of the CFON surface. The observed decrease in adsorption efficiency at elevated temperatures may be attributed to several factors. The greater kinetic energy of dye molecules at higher temperatures means less residence time is available for them near the surface of the adsorbent. The best adsorption results at 30 °C hint that cooler temperatures are more favorable for AR73 dye removal, making CFON more useful in normal or close-to-normal conditions. Correspondingly, the thermodynamic parameters in Table 4S showed the positive value of enthalpy change ($\Delta H^o$) (56.99 kJ $mol^{-1}$), confirming the exothermic nature of the adsorption process. This means the adsorption process releases heat, making lower temperatures more favorable. The negative value of entropy change ($\Delta S^o$) (-0.154 J $mol^{-1}$ $K^{-1}$) suggests a decrease in randomness at the solid/liquid interface during adsorption. This could be due to the ordered arrangement of dye molecules on the adsorbent surface (Ali & Alrafai, 2016). The negative values of Gibbs free energy change ($\Delta G^o$ < -10 kJ $mol^{-1}$) indicate that the adsorption process is spontaneous at all temperatures investigated. The constant value of $\Delta G^o$ across the temperature range suggests that the driving force for adsorption remains consistent despite the changing temperature (Şentürk, 2024). The negative value of $\Delta G^o$ (< -10 kJ $mol^{-1}$) suggests that the dominant mechanism is physical adsorption, involving weak forces of attraction, such as van der Waals forces, hydrogen bonding, and electrostatic interactions. This mechanism is further supported by the positive $\Delta H^o$ value, indicating that the adsorption process is driven by the release of heat (Abualnaja *et al.*, 2021).

### 3.6. Reusability of The Adsorbent Material:

A 50 mg/L solution of AR73 dye was used in the current study to evaluate the composite's reusability through a series of adsorption-desorption cycles. To replicate realistic operating parameters, the experimental conditions included agitation at 180 rpm for four hours (Supplementary Figure 4). With an impressive 98.160% dye removal efficiency during the first adsorption cycle (R1), the composite demonstrated a high binding affinity between the dye molecules and the adsorbent surface. Efficiency dropped to 88.7% in the second cycle (R2), indicating a moderate decline in performance. The composite's significant removal capacity, which reflects its structural stability and reusability, persisted despite this decline (Misran *et al.*, 2022). Nevertheless, the third cycle (R3) showed a significant decrease in adsorption efficiency, with removal efficiency plummeting to 9.99%. This notable decrease points to a noticeable decline in the adsorbent's surface functionality or active sites following repeated use (Fouda-Mbanga *et al.*, 2024). Over the first two cycles, the composite exhibited encouraging reusability; however, the third cycle revealed limitations that could be attributed to saturation of the adsorption sites, structural fatigue, or possible surface chemical changes. These results highlight that, while the composite is initially efficient and partially reusable, regeneration techniques or material reinforcement may be necessary for long-term use to maintain high performance. When considering its implementation in continuous or large-scale treatment systems, it is important to consider the decline observed in subsequent cycles (Egbosiuba *et al.*, 2024).

### 3.7. Comparative Adsorption Performance of $Fe_2O_3$ Nanoparticles for Various Dyes:

Table 4 summarizes the adsorption capacities and removal efficiencies of $Fe_2O_3$ nanoparticles reported in previous studies for different dyes, alongside the current study's results for AR73. As shown, the $Fe_2O_3$ nanoparticles exhibit varying adsorption capacities depending on the dye type, with the present research achieving a notably high adsorption capacity of 357.14 mg/g for AR73. This demonstrates the superior performance of the synthesized $Fe_2O_3$ nanocomposite in removing AR73 compared to other dyes reported in the literature. The comparison highlights the effectiveness and potential applicability of $Fe_2O_3$-based materials in dye removal from aqueous solutions.

**Table 4: Comparison study for $Fe_2O_3$-NPs for the removal of different dyes.**

| Dye | The highest dye adsorption Capacity or percentage removal | References |
|---|---|---|
| **Maxilon blue GRL** | 0.23 mg/g | (Yakar *et al.*, 2020) |
| **Navy blue** | 49.3% | (Yakar *et al.*, 2020) |
| **Safranin** | 66% | (Hammad *et al.*, 2022) |
| **Cationic crystal violet** | 256.4 mg/g | (Shalaby *et al.*, 2021) |
| **Anionic methyl orange** | 270.2 mg/g | (Shalaby *et al.*, 2021) |
| **Methyl orange** | 81% | (Beheshtkhoo *et al.*, 2018) |
| **Coomassie brilliant blue R-250** | 0.306 mol/g & (98%) | (Chaudhary *et al.*, 2013) |
| **AR73** | 357.14 mg/g | This study |

## 4. Conclusion

This study successfully demonstrated the exceptional ability of a chitosan/ferrous oxide nanocomposite (CFON) in removing AR73 dye from aqueous solutions. Additionally, the removal efficiency and adsorption capacity increased with longer contact times, achieving near-complete removal. Besides, elimination efficiency initially increased with higher dye concentrations but plateaued at higher concentrations. Adsorption capacity consistently increased with higher initial concentrations. The optimization of process parameters using RSM further enhanced the practicality and effectiveness of the nanocomposite for dye removal applications. The RSM model, despite a high $R^2$ value, lacked statistical significance in explaining the variation in dye removal efficiency. The interaction between contact time and pH had the most substantial impact on removal efficiency. 3D response surface plots highlighted the complex interplay between factors and the need for optimization, considering all relevant parameters. Additionally, the positive impact on water quality parameters in aquaculture settings highlights the potential of this material for broader environmental remediation purposes. This work offers valuable insights into the development of efficient and environmentally friendly adsorbents for wastewater treatment, addressing the pressing issue of dye pollution.

**Study Limitations:** Despite the high $R^2$ value, the RSM model used in the study lacked statistical significance, limiting its predictive reliability for optimizing dye removal. The adsorption mechanism was not fully elucidated, with the specific roles of FeO nanoparticles and different interaction types (e.g., hydrogen bonding, electrostatic interactions) remaining unclear. The investigation was restricted to a single anionic dye (AR73) in simple aqueous solutions, without evaluating performance in real wastewater or in the presence of competing contaminants. Moreover, no regeneration strategies were explored, and the sharp decline in adsorption efficiency by the third reuse cycle poses challenges for long-term application. Issues related to large-scale synthesis, material formulation, and economic feasibility were not addressed.

Future Recommendations: Further research should focus on optimizing the FeO nanoparticle content within the chitosan matrix to balance adsorption performance with structural and functional stability. Enhancing the RSM model through expanded experimental design or integrating it with advanced modeling techniques such as artificial neural networks could improve predictive accuracy and mechanistic insight. Investigating effective regeneration methods would increase material reusability and economic viability. The material's effectiveness should also be tested against a broader range of pollutants, including cationic dyes, heavy metals, and pesticides, as well as in real or synthetic wastewater environments. Finally, efforts should be made to scale up the synthesis process, develop practical adsorbent forms (e.g., beads, membranes), perform techno-economic assessments, and evaluate the feasibility of combining adsorption with catalytic degradation for improved overall treatment performance. Transitioning to column-based continuous flow systems would also better simulate real-world operating conditions and support commercial applicability.

## Data Availability Statement

The data that support the findings of this study are available within the article and/or its supplementary materials. The author can provide further details with reasonable requests.

## Acknowledgments

The author extends sincere appreciation to Taif University, Saudi Arabia, for its support and encouragement during this research.

## Funding

No funding was received for this research.

## Conflicts of Interest

The author states that there is no conflict of interest. The author declares no financial or non-financial competing interests.

## Biographies

**Khamael M. Abualnaja**

*Department of Chemistry, College of Science, Taif University, Taif 21944, Saudi Arabia, 00966543362333, k.ala@tu.edu.sa*

Prof. Khamael is a Saudi Arabian scholar whose research centers on physical chemistry and its integration with mathematical modeling, particularly in the fields of numerical analysis, differential equations, and environmental applications. She has published extensively in international journals and is widely recognized for her interdisciplinary collaborations. With deep expertise in theoretical modeling and numerical simulations, she makes significant contributions to scientific advancement through innovative research and leadership in academia.

ORCID: 0000-0001-9555-5380

## References

Abdallah, M.A.M. and Alprol, A.E. (2024). Utilization of aquatic biomass as biosorbent for sustainable production of high surface area, nano-microporous, for removing two dyes from wastewater. *Scientific Reports*, **14**(1), 4471. DOI: 10.1038/s41598-024-54539-2.

Abualnaja, K.M., Alprol, A.E., Ashour, M. and Mansour, A.T. (2021). Influencing multi-walled carbon nanotubes for the removal of ismate violet 2R dye from wastewater: isotherm, kinetics, and thermodynamic studies. *Applied Sciences*, **11**(11), 4786. DOI: 10.3390/app11114786.

Akhtar, K., Khan, S.A., Khan, S.B. and Asiri, A.M. (2018). Scanning Electron Microscopy: Principle and Applications in Nanomaterials Characterization. In: Sharma, S. (eds) *Handbook of Materials Characterization*. Springer, Cham. DOI: 10.1007/978-3-319-92955-2_4.

Alprol, A. (2019). Study of environmental concerns of dyes and recent textile effluents treatment technology: A review. *Asian J. Fish. Aquat. Res*, **3**(2), 1–18. DOI: 10.9734/ajfar/2019/v3i230032.

Alprol, A.E., Mansour, A.T., Abdelwahab, A.M. and Ashour, M. (2023). Advances in green synthesis of metal oxide nanoparticles by marine algae for wastewater treatment by adsorption and photocatalysis techniques. *Catalysts*, **13**(5), 888. DOI: 10.3390/catal13050888.

Alprol, A.E., Mansour, A.T., Ibrahim, M.E.E.D. and Ashour, M. (2024). Artificial intelligence technologies revolutionizing wastewater treatment: Current trends and future prospective. *Water*, **16**(2), 314. DOI: 10.3390/w16020314.

Ashour, M., Alprol, A.E., Khedawy, M., Abualnaja, K.M. and Mansour, A.T. (2022). Equilibrium and kinetic modeling of crystal violet dye adsorption by a marine diatom, skeletonema costatum. *Materials*, **15**(18), 6375. DOI: 10.3390/ma15186375.

Ashour, M., Mansour, A.T., Abdelwahab, A.M. and Alprol, A.E. (2023). Metal oxide nanoparticles' green synthesis by plants: Prospects in phyto- and bioremediation and photocatalytic degradation of organic pollutants. *Processes*, **11**(12), 3356. DOI: DOI: 10.3390/pr11123356.

Banerjee, S., Mukherjee, S., LaminKa-Ot, A., Joshi, S., Mandal, T. and Halder, G. (2016). Biosorptive uptake of $fe^{2+}$, $cu^{2+}$ and $as^{5+}$ by activated biochar derived from colocasia esculenta: Isotherm, kinetics, thermodynamics, and cost estimation. *Journal of Advanced Research*, **7**(5), 597–610. DOI: 10.1016/j.jare.2016.06.002.

Chaleshtori, A.N., Meghadddam, F.M., Sadeghi, M., Rahimi, R., Hemati, S. and Ahmadi, A. (2017). Removal of acid red 18 (azo-dye) from aqueous solution by adsorption onto activated charcoal prepared from almond shell. *Journal of Environmental Science and Management*, **20**(2), 9–16. DOI: 10.47125/jesam/2017_2/02.

Chueachot, R., Wongkhueng, S., Khankam, K., Lakrathok, A., Kaewnon, T., Naowanon, W., Amnuaypanich, S. and Nakhowong, R. (2018). Adsorption efficiency of methylene blue from aqueous solution with amine-functionalized mesoporous silica nanospheres by co-condensation biphasic synthesis: Adsorption condition and equilibrium studies. *Materials Today: Proceedings*, **5**(6), 14079–85. DOI: 10.1016/j.matpr.2018.02.066.

Fan, J., Guo, Y., Wang, J. and Fan, M. (2009). Rapid decolorization of azo dye methyl orange in aqueous solution by nanoscale zerovalent iron particles. *Journal of Hazardous Materials*, **166**(2-3), 904–10. DOI: 10.1016/j.jhazmat.2008.11.091.

Freundlich, H.M.F. (1906). Over the adsorption in solution. *Journal of Physical Chemistry*, **57**(385471), 1100–7.

Ghoneim, M.M., El-Desoky, H.S., El-Moselhy, K.M., Amer, A., Abou El-Naga, E.H., Mohamedein, L.I. and Al-Prol, A.E. (2014). Removal of cadmium from aqueous solution using marine green algae, Ulva lactuca. *The Egyptian Journal of Aquatic Research*, **40**(3), 35–242. DOI: 10.1016/j.ejar.2014.08.005.

Harkins, W.D. and Jura, G. (1943). An adsorption method for the determination of the area of a solid without the assumption of a molecular area, and the area occupied by nitrogen molecules on the surfaces of solids. *The Journal of Chemical Physics*, **11**(9), 431–2. DOI: 10.1063/1.1723871.

Kareem, F.F., M.F.H. Al-Kadhemy, and A.A. Saeed. (2021). Impact of solvents, magnesium oxide and aluminium oxide nanoparticles on the photophysical properties of acridine orange dye. *Scientific Journal of King Faisal University: Basic and Applied Sciences*, **22**(2), 113–9. DOI: 10.37575/b/sci/210047.

Karimifard, S. and Moghaddam, M.R.A. (2018). Application of response surface methodology in physicochemical removal of dyes from wastewater: A critical review. *Science of the Total Environment*, **640**(n/a), 772–97. DOI: 10.1016/j.scitotenv.2018.05.355.

Karri, R.R. and Sahu, J. (2018). Modeling and optimization by particle swarm embedded neural network for adsorption of zinc (ii) by palm kernel shell based activated carbon from aqueous environment. *Journal of Environmental Management*, **206**(n/a), 178–91. DOI: 10.1016/j.jenvman.2017.10.026.

Kasraee, M., Dehghani, M.H., Hamidi, F., Mubarak, N.M., Karri, R.R., Rajamohan, N. and Solangi, N.H. (2023). Adsorptive removal of acid red 18 dye from aqueous solution using hexadecyl-trimethyl ammonium chloride modified nano-pumice. *Scientific Reports*, **13**(1), 13833. DOI: 10.1038/s41598-023-41100-w.

Krishnan, K.A. and Haridas, A. (2008). Removal of phosphate from aqueous solutions and sewage using natural and surface modified coir pith. *Journal of Hazardous Materials*, **152**(2), 527–35. DOI: 10.1016/j.jhazmat.2007.07.015.

Langmuir, I. (1916). The constitution and fundamental properties of solids and liquids. Part i. Solids. *Journal of the American Chemical Society*, **38**(11), 2221–95. DOI: 10.1021/ja02268a002.

Mansour, A.T., Alprol, A.E., Abualnaja, K.M., El-Beltagi, H.S., Ramadan, K.M.A. and Ashour, M. (2022a). The using of nanoparticles of microalgae in remediation of toxic dye from industrial wastewater: Kinetic and isotherm studies. *Materials (Basel)*, **15**(11), 3922. DOI: DOI: 10.3390/ma15113922.

Mansour, A.T., Alprol, A.E., Ashour, M., Ramadan, K.M.A., Alhajji, A.H.M. and Abualnaja, K.M. (2022b). Do red seaweed nanoparticles enhance bioremediation capacity of toxic dyes from aqueous solution? *Gels*, **8**(5), 310. DOI: 10.3390/gels8050310.

Mukherjee, D., Ghosh, S., Majumdar, S. and Annapurna, K. (2016). Green synthesis of α-fe2o3 nanoparticles for arsenic (v) remediation with a novel aspect for sludge management. *Journal of Environmental Chemical Engineering*, **4**(1), 639–50. DOI: 10.1016/j.jece.2015.12.010.

Preethi, S., Abarna, K., Nithyasri, M., Kishore, P., Deepika, K., Ranjithkumar, R., Bhuvaneshwari, V. and Bharathi, D. (2020). Synthesis and characterization of chitosan/zinc oxide nanocomposite for antibacterial activity onto cotton fabrics and dye degradation applications. *International Journal of Biological Macromolecules*, **164**(n/a), 2779–87. DOI: 10.1016/j.ijbiomac.2020.08.047.

Putra, W.P., Kamari, A., Yusoff, S.N.M., Ishak, C.F., Mohamed, A., Hashim, N. and Isa, I.M. (2014). Biosorption of cu (ii), pb (ii) and zn (ii) ions from aqueous solutions using selected waste materials: Adsorption and characterisation studies. *Journal of Encapsulation and Adsorption Sciences*, 4(1), 25–35. DOI: 10.4236/jeas.2014.41004.

Raval, N.P., Shah, P.U. and Shah, N.K. (2017). Malachite green "a cationic dye" and its removal from aqueous solution by adsorption. *Applied Water Science*, **7**(n/a), 3407–45. DOI: 10.1007/s13201-016-0512-2.

Ravulapalli, S. and Kunta, R. (2019). Effective removal of methylene blue, a hazardous dye from industrial effluents using active carbon of F. infectoria plant. *International Journal of Environmental Science and Technology*, **16**(12), 7837–48. DOI: 10.1007/s13762-018-2147-3.

Salazar-Rabago, J.J., Leyva-Ramos, R., Rivera-Utrilla, J., Ocampo-Perez, R. and Cerino-Cordova, F.J. (2017). Biosorption mechanism of methylene blue from aqueous solution onto white pine (Pinus durangensis) sawdust: Effect of operating conditions. *Sustainable Environment Research*, **27**(1), 32–40. DOI: 10.1016/j.serj.2016.11.009.

Yan, H., Yang, H., Li, A. and Cheng, R. (2016). PH-tunable surface charge of chitosan/graphene oxide composite adsorbent for efficient removal of multiple pollutants from water. *Chemical Engineering Journal*, **284**(n/a), 1397–405. DOI: 10.1016/j.cej.2015.06.030.

## Copyright